Proceedings of the American Control Conference
San Diego, California • June 1999

Dual-Stage Track-Following Servo Design for Hard Disk Drives [1]

Daniel Hernandez[2], Sung-Su Park[3], Roberto Horowitz[4], Andrew K. Packard[5]
Department of Mechanical Engineering
University of California, Berkeley, CA 94720-1740

Abstract

Discrete time, 25 KTPI track-following servos were designed for magnetic hard disk drive dual stage actuators using the μ-synthesis methodology. The design methodology was tested on two microactuator models. The first is a model of a piezoelectrically actuated suspension, currently under development by Hutchinson Technology Incorporated (HTI). The second is a model of an electrostatically actuated MEMS microactuator, currently under development by the IBM Almaden Research Center. Low order controllers were successfully designed for both models, which achieved the prescribed robustness and performance requirements.

1 Introduction

Magnetic Hard Disk Drive (MHDD) storage technology continues to experience a dramatic areal density growth of 60% per year. At this rate, it is projected that MHDD products will have areal densities of 10 Gbit/in^2 and 40 Gbit/in^2 by the years 2001 and 2004 respectively [1]. It has been estimated that a track density of 25,000 tracks-per-inch (25KTPI) will be required to achieve 10 Gbit/in^2. This will in turn require and approximate servo bandwidth of 2.5 kHz, if one extrapolates the bandwidth requirements of current 3.5" HDD products. Because conventional servo actuators cannot provide this level of tracking accuracy, the use of a microactuator for high-bandwidth, high accuracy positioning has been proposed. Two approaches to microactuation are currently being considered. The first may be described as an actuated suspension. In this approach, conventional assembly and machining techniques are used to integrate an electromagnetic or piezoelectric actuator into a steel suspension [2, 3]. The second approach consists in placing a microactuator in between the slider and the gimbal of the suspension [4, 5]. The microactuators used in these schemes are generally fabricated using MEMS fabrication techniques and are actuated by either piezoelectric, electromagnetic or electrostatic forces. These systems potentially offer increase performance at reduced costs, due to the use and integration of large scale and high volume MEMS fabrication technologies. Moreover, these microactuators may incorporate means of measuring the motion of the slider relative to the suspension. However, these actuators are still under development and their incorporation into actual products will require relatively large capital investments by the magnetic recording industry.

In this paper we discuss the design of dual-stage servos using μ-synthesis [6, 7]. Two piggy-back actuator designs will be considered. The first is a piezoelectrically driven actuated suspension, currently under development by Hutchinson Technology Incorporated (HTI) [2]. The second is an electrostatically driven MEMS based Invar microactuator, currently under development by the IBM Almaden Research Center [4]. Dual-stage servos capable of attaining 25 KTPI, will be presented for these two systems.

[1] Research partially supported by the National Storage Industrial Consortium (NSIC), DARPA Grant DABT63-95-C-0028, and the UC Berkeley Computer Mechanics Laboratory (CML)

[2] Graduate student. Presently at Voyan Technology, Santa Clara, CA, dhernandez@voyan.com.
[3] Graduate student; spark@me.berkeley.edu.
[4] Professor; horowitz@me.berkeley.edu.
[5] Professor; pack@me.berkeley.edu.

2 Dual-Stage Actuator Models

IBM has disclosed an electrostatically actuated invar microactuator which is assembled between the slider and the gimbal of the suspension [4]. The microactuator is a rotational structure which is driven by electrostatic comb drives and rotates the slider relative to the suspension. The current demonstration design attains a head stroke displacement of 2 μm. A typical voltage swing of 60 volts (or +-30V) is required. However, future high-efficiency efficient microactuator designs, operating under +- 20V are possible. The microactuator has a lightly damped resonance mode at 1.5 kHz. Because the microactuator is designed to rotate the slider relative to its center of mass, the coupling dynamics between the coarse actuator and the microactuator can be neglected. The block diagram used to describe the IBM dual-stage system is shown in Fig 1 v_{VCM} in

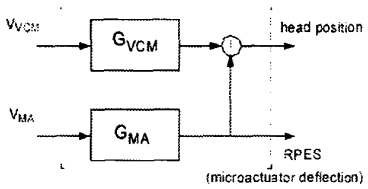

Figure 1: IBM and HTI Model Block Diagram

Fig. 1 is the input voltage to the voice coil motor (VCM), v_{MA} is the voltage input to the microactuator, $G_{VCM}(s)$ is the transfer function which describes the coarse actuator dynamics, including the Voice Coil Motor (VCM) and suspension dynamics. $G_{MA}(s)$ is the microactuator transfer function. Fig. 2 shows the gain Bode plots for $G_{VCM}(j\omega)$ and $G_{MA}(j\omega)$ for the IBM dual-stage system, as well as the model uncertainty weightings that will be used in the μ-synthesis design. It should be noted that, because of etching process variations, the microactuator's resonance frequency can vary by as much as $\pm 10\%$ from one actuator to another.

HTI has disclosed a piezoelectrically based microactuator located in the suspension load beam [2]. The design utilizes two PZT elements, which respectively expand and contract when a voltage potential is applied across their thickness, working together to rotate the load beam and producing a slider off track motion. The current design attains a stroke displacement of 2 μm for a maxi-

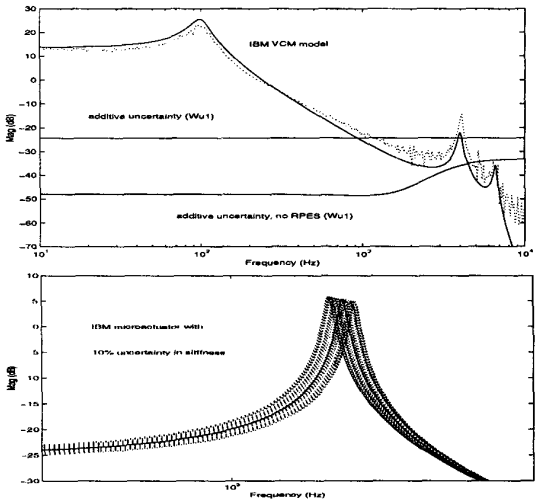

Figure 2: Bode plots of IBM dual-stage model

mum input voltage of 42 Volts. The microactuator has a first resonance mode of 5.5 kHz. This design has both advantages and disadvantages. First, the control system does not have collocated sensing and control, as in the electrostatic MEMS designs. Control is applied at the base of the suspension. However, the PES is read by the head at the tip of the suspension. The suspension has many resonance modes and, in addition, the motion of the read/write heads is also coupled to the motion of the coarse actuator through the modes of the piezoelectric films. Second, no relative position sensing of the microactuator is available for the active suspension. On the other hand, the piezo-actuator has a relatively high resonant frequency at about 5.5 kHz. As will be seen later, measurements of the microactuators displacement are less important if the bandwidth of the microactuator is well beyond the desired closed-loop bandwidth of 2 kHz. In this case the microactuator is working mainly in the low-frequency, DC gain section of its frequency response, and is less sensitive to perturbations in the model. Fig. 1 also describes the block diagram used to model the HTI dual-stage system in this paper. In this paper we utilize transfer functions obtained from HTI to perform our controller design. It should be noted that the model used by HTI neglects the excitation of other suspension resonance modes by the piezoelectric actuator (except for its own 5.5 kHz resonance mode). Fig. 3 shows the gain Bode plots for $G_{VCM}(j\omega)$ and $G_{MA}(j\omega)$ used to model the HTI dual-stage system, as well

as the model uncertainty weightings that will be used in the μ-synthesis design.

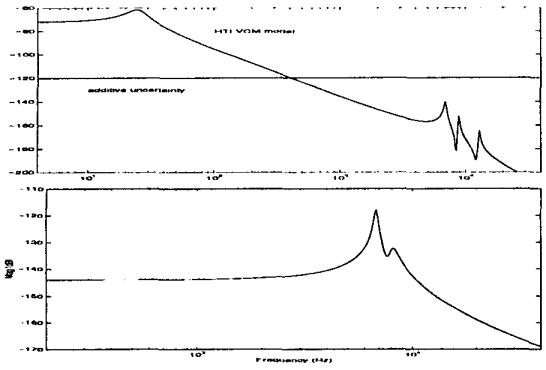

Figure 3: Bode Plots of HTI Dual-stage model

3 μ-Synthesis Design Methodology

The μ-synthesis block diagram used in the design of the dual-stage servo controller is shown in Fig. 4. The block diagram contains many signals and weightings that allow for a fairly complete description of a dual-stage HDD environment. Let P be the nominal plant model of the system comprised of the coarse and fine actuators. Independent multiplicative or additive uncertainties can be used to describe uncertainty for both the coarse actuator and microactuator (additive uncertainties are shown in Fig.4). In addition, a 10% parametric uncertainty on the spring stiffness of the microactuator is incorporated in the design for the IBM model.

Several disturbance signals are accounted for in the model, including the track runout r, input disturbances to the coarse and fine actuators, d_{VCM} and d_{MA} respectively, the head Position Error Signal (PES) sensor noise n_{PES} and the microactuator Relative Position Error Signal(RPES) sensor noise n_{RPES}. In the synthesis model in Fig. 4 these disturbance signals are generated by passing normalized signals (i.e. signals with infinity norm less than or equal to one) $\overline{r}$, $\overline{d_{VCM}}$, $\overline{d_{MA}}$, $\overline{n_{PES}}$ and $\overline{n_{RPES}}$ respectively thru weightings W_R, W_{DVCM}, W_{DMA}, W_{NPES} and W_{NRPES}, which can be either constants or frequency shaping filters. These weightings must be selected by the designer so that disturbances are modeled with sufficient fidelity.

The output signals in the synthesis model are the head Position Error Signal (PES), the microactuator's Relative Position Error Signal (RPES) and the VCM and microactuator control inputs u_{VCM} and u_{MA} respectively. These signals are respectively multiplied by scaling factors W_{PES}, W_{RPES}, W_{uVCM}, W_{uMA} to produce the performance output signals $\overline{PES}$, $\overline{RPES}$, $\overline{u_{VCM}}$ and $\overline{u_{MA}}$. The scaling factors must be selected so that, the output signal reaches its specified upper bound when its corresponding performance output is equal to 1.

Given a set of input and output weightings and plant uncertainties, if the μ-synthesis methodology is successful and a controller is synthesized which has a μ value less than or equal to 1, than the transfer function, $\overline{T}$, from the normalized disturbances

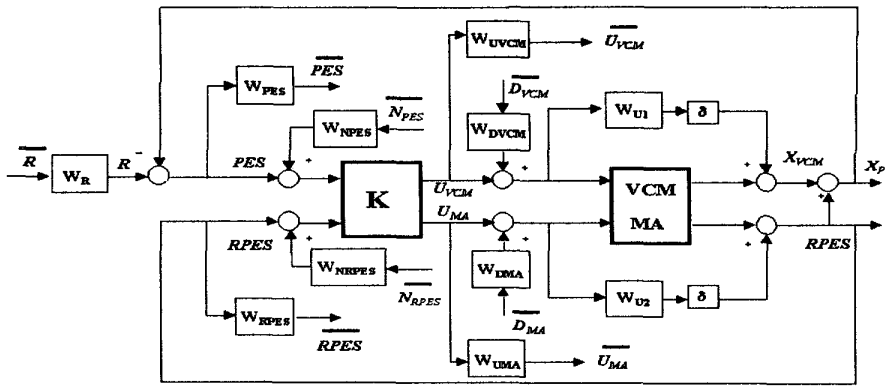

Figure 4: μ-Synthesis design block diagram

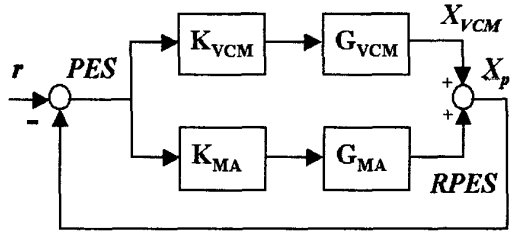

Figure 5: SIMO track following servo

$$\overline{d} = (\overline{R}, \overline{d_{VCM}}, \overline{d_{MA}}, \overline{n_{PES}}, \overline{n_{RPES}}) \quad (1)$$

to the weighted performance signals

$$\overline{e} = (\overline{PES}, \overline{RPES}, \overline{u_{VCM}}, \overline{u_{MA}}), \quad (2)$$

will have infinity norm less than or equal to 1 for all uncertainties $|\delta_i| \leq 1$ and robust stability,i.e.,

$$\mu(F_U(K, F_L(P, \Delta))) \leq 1 \Rightarrow ||\overline{T}||_\infty \leq 1$$

See [6] for details. An interpretation of this result which is useful for design purposes is as follows. Assume that each element $\overline{d}_i$ of the disturbance input vector in Eq. (1) is a sinusoidal of the form $\overline{d}_i(t) = \overline{D}_i \sin(\omega t + \psi_i)$, such that $\sum_{i=1}^{s} D_i^2 \leq 1$. Then the steady state response of each element $\overline{e}_i$ of the performance signal vector $\overline{e}$ in Eq. (2) will also be a sinusoidal of the form $\overline{e_{ss}}_i(t) = E_i \sin(\omega t + \phi_i)$, where $E_i \leq 1$, $i = 1 \cdots 4$. For design purposes we often approximate $\sum_{i=1}^{s} D_i^2 \leq 1$ by the less conservative statement $D_i \leq 1$, $i = 1 \cdots 5$.

4 Controller Designs

Three discrete time track-following servos were designed. The first is a SIMO 25 kHz sampling rate controller for the HTI dual-stage actuator model. In this design the head Position Error Signal (PES) is fed to both the microactuator and the VCM compensators, as shown Fig. 5. X_P in Fig. 5 represents the magnetic head absolute position, X_{VCM} the slider tip absolute position and r the position of the track center. K_{VCM} and K_{MA} are respectively VCM and microactuator compensators. An equivalent block diagram representation of the SIMO design is shown in Fig. 6. Notice that

$$\begin{aligned} PES &= r - X_P\,, \quad PES_{VCM} = r - X_{VCM} \\ RPES &= X_P - X_{VCM}\,. \end{aligned} \quad (3)$$

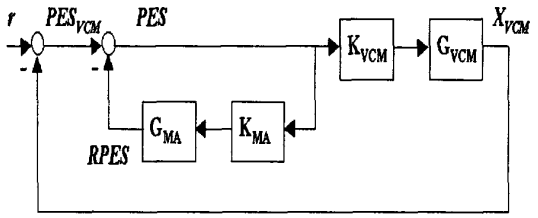

Figure 6: Equivalent SIMO representation

Two discrete time 20 KHz dual-stage controllers were designed for the IBM dual-stage actuator model, a SIMO design with block diagram given by Figs. 5 and 6, and a MIMO design in which both the PES and $RPES$ are fed to the control system.

Table 1 shows the weights used in the μ-synthesis block diagram in Fig. 4, for the three designs. Fig. 7 shows the magnitude Bode plot of the filters, W_R, used to characterized track runout. The filter used in the designs for the IBM model was curved fitted from data obtained from and actual 3.5" drive. The one used in the design for the HTI model was synthesized by extrapolating current performance specifications. All frequency weightings were approximated by digital filters using the Tustin transformation with pre-warping. HDD servo systems

Weight	HTI	IBM	
	SIMO	SIMO	MIMO
W_R	Fig. 7	Fig. 7	Fig. 7
W_{DVCM}	0.45 mV	0.058 mA	0.058 mA
W_{DMA}	23 mV	1.8 V	1.8 V
W_{NPES}	10 nm	6.5 nm	6.5 nm
W_{NRPES}	-	-	8 nm
W_{PES}	1/(80 nm)	1/(127 nm)	1/(100 nm)
W_{RPES}	1/(2 μm)	1/(2 μm)	1/(2 μm)
W_{UVCM}	1/(2 A)	1/(360 mA)	1/(360 mA)
W_{UMA}	1/(100 V)	1/(30 V)	1/(30 V)
W_{U1A}	Fig. 3	Fig. 2	Fig. 2
W_{U2A}	-	1.3 nm/V	1.3 nm/V

Table 1: Fig. 4 Weightings

are generally designed so that three times the statistical standard deviation (3σ) of the Track Mis-Registration (TMR) is within 1/10 of the track-to-track pitch. Thus, a 3σ TMR of 0.1 μ m is required for a 25 KTPI tracking density. This performance

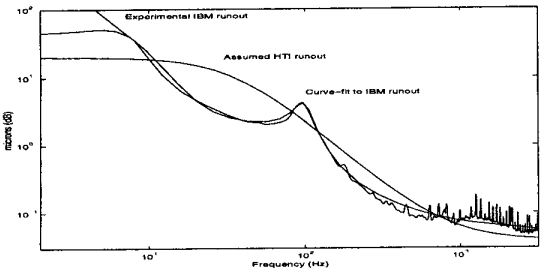

Figure 7: Frequency response of W_R filters

specification can be enforced in the μ-synthesis framework by requiring that $|PES| \leq 0.1\mu m$ for all disturbances $||\overline{d}(t)|| < 1$ in Eq. (1) . Thus, weights $W_{PES} \approx 1/(0.1\mu m)$ in Fig. 4 were chosen in all three designs[1]. Likewise, $W_{RPES} = 1/(2\mu m)$ was selected to guarantee that the manipulator stroke would not exceed 2 μm in all designs. The VCM open loop gain crossover frequency (e.g. the gain of the transfer function $X_p(z)/PES_{VCM}(z)$ in Fig. 6) was adjusted with the additive uncertainties weights W_{U1A} in Fig. 4. Roughly, the VCM open loop gain crossover frequency occurs at the frequency where the gain of the additive uncertainty is equal to the gain of the transfer function G_{VCM} (Figs. 2 and 3). A microactuator multiplicative uncertainty $W_{U2M} = 0.005 \frac{10^4}{500} \frac{s+2\pi 500}{s+2\pi 10^4}$ was used in the design for the HTI actuator, while additive uncertainties (shown in table 1) were used in the designs for the IBM actuator. As stated earlier, 10% variation in the microactuator resonance frequency was imposed in the IBM μ-synthesis block diagram using a stiffness parametric uncertainty. Weight W_{UMA} were used to bound the microactuator input voltage within prescribed values. However, in the case of the HTI model, W_{UMA} was decreased to 1/(100 V) in light of the fact that the initial design results using $W_{UMA} = 1/(40V)$ were too conservative. The weights W_{DVCM}, W_{DMA}, W_{NPES} and W_{NRPES} in table 1 were determined by extrapolating the PES decomposition results presented by [8]. $W_{NPES} = \sqrt{2} * 0.32\%$ of a track was used to generate PES noise, where the $\sqrt{2}$ factor was included in the expression to account for the fact that the H-infinity framework is deterministic and disturbances are estimated based on the RMS values of sinusoids rather than stochastic signals.

[1]Weights differed slightly in some cases to relax the conservativeness of the resulting design.

5 Simulation Results

The μ-synthesis toolbox synthesized discrete times controllers that achieved $\mu < 1$ for all three dual-stage designs with the performance and plant uncertainty specifications described in the previous section. The order of the controllers was successfully reduced in all three cases, yielding a ninth order controller for the HTI model, and respectively tenth and twelfth order MIMO and SIMO controllers for the IBM model. These controllers also achieved $\mu < 1$. Fig. 8 shows the gain Bode plot of the error rejection closed loop transfer function ($r(z)$ to $PES(z)$) for all three designs. Notice

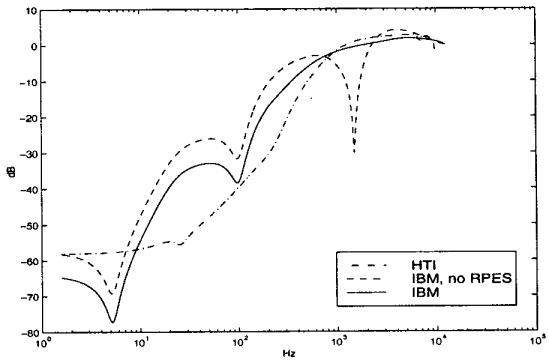

Figure 8: Error rejection transfer frequency response

that the differences between the middle to low frequency portion of the Bode Plots in Fig. 8 is mainly due to the fact that different filters W_R were used to characterized the runout r in the two models. All three designs have a bandwidth in the 1-2 kHz frequency range. Recall that the IBM model has a lightly damped resonance mode at around 1.5 kHz, which may vary in frequency by as much as 10 % from actuator to actuator. The poles of this resonance mode were damped and placed at a lower frequency by the MIMO controller. Pole placement can be accomplished robustly in this design because the RPES is assumed to be measurable. The SIMO controller did not exactly cancel this resonance mode via a notch filter, as evidenced by the sharp notch in the SIMO error rejection response at that frequency. This was due to the fact that the controller was required to perform robustly under a 10 % frequency variation of this mode. In contrast, the HTI model has its first resonance mode

at around 5.5 kHz, and no frequency uncertainty in this mode was assumed. As a consequence, the SIMO controller for the HTI system can effectively notch this mode. Fig. 9 shows a PES time response for a simulated 1 μm step response for all three designs. Finally, Fig. 10 shows open loop

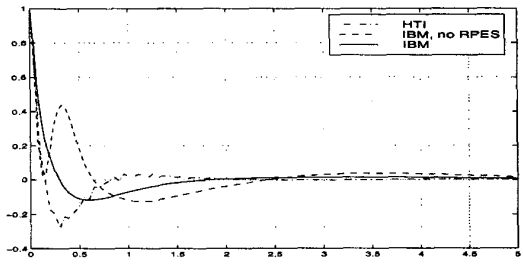

Figure 9: 1 μm step input response (time in msec)

Bode plots for the HTI SIMO controller ($PES(z)$ to $X_P(z)$ in Fig. 5 and $PES_{VCM}(z)$ to $X_{VCM}(z)$ in Fig. 6). These plots reveal that the control system effectively limits the high frequency response of the VCM, while achieving an overall bandwidth in excess of 1 kHz.

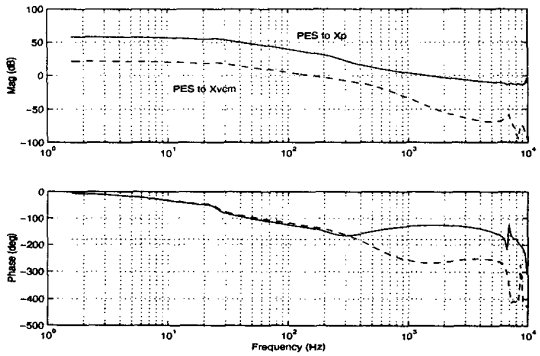

Figure 10: Open loop Bode plots for the HTI SIMO controller

6 Conclusion

Discrete time, 25 kTPI track-following servos were designed for magnetic hard disk drive dual stage actuators using the μ-synthesis methodology. The methodology was tested on a piezoelectrically actuated suspension model, with a first order resonance mode at 5.5 kHz, and a MEMS electrostatic microactuator model, with a lightly damped resonance mode at 1.5 kHz. Low order controllers were successfully designed for both models, which achieved the prescribed robustness and performance requirements. In the case of the MEMS electrostatic microactuator, two controller designs were tested. The first is a SIMO control system, in which the head PES is fed to both the VCM and microactuator compensators. The second is a MIMO control system, in which both the head PES and the microactuator RPES are directly measured by the control system. Simulation results reveal that direct measurement of the microactuator RPES allows the MIMO control system to robustly damp the microactuator's resonance poles and placed them at a lower frequency, enhancing the robustness of the overall control system, as compared to the SIMO design.

References

[1] Grochowski and R. Hoyt, "Future trends in hard disk drives," *IEEE Transactions on Magnetics*, vol. 32, pp. 1850–1854, May 1996.

[2] R. Evans, J. Griesbach, and W. Messner, "Piezoelectric microactuator for dual stage control," in *Digests of the Asia Pacific Magnetic Recording Conference (APMRC)*, July 1998. To appear in the IEEE Transactions on Magnetics (March 1999).

[3] S. Konagezawa, Y. Uematsu, and T. Yamada, "Dual-stage actuator system for magnetic disk drives using shear mode piezoelectric microactuator," in *Digests of the APMRC*, July 1998. To appear in the IEEE Transactions on Magnetics (March 1999).

[4] T. Hirano, L.-S. Fan, W. Y. Lee, J. Hong, W. Imaino, S. Pattanaik, S. Chan, P. Webb, R. Horowitz, S. Aggarwal, and D. Horsley, "High-bandwidth, high-accuracy rotary microactuators for magnetic disk drives tracking servos," *IEEE/ASME Transactions on Mechatronics*, vol. 3, September 1998.

[5] D. Horsley, R. Horowitz, and A. Pisano, "Microfabricated microactuators for hard disk drives," *IEEE/ASME Transactions on Mechatronics*, vol. 3, September 1998.

[6] G. Balas, J. Doyle, K. Glover, A. Packard, and R. Smith, "μ-analysis and synthesis toolbox," 1995. MUSYN and Mathworks Inc.

[7] S. Aggarwal, D. Horsley, R. Horowitz, and A. Pisano, "Microactuators for high density disk drives," in *Proceedings of the American Control Conference*, 1997. Albaquerque, New Mexico, USA.

[8] R. Ehrlich and D. Curran, "Major HDD TMR sources, and projected scaling with TPI," in *Digests of the APMRC*, July 1998. To appear in the IEEE Transactions on Magnetics (March 1999).